

Article

Influence of Replacing Molybdenum with Tungsten on the Creep Fracture Property of Waspaloy Nickel-Based Alloy

Hanxin Yao ^{1,2,*}, Jianxin Dong ^{1,*}, Zhihua Gong ^{3,4} , Jiqing Zhao ⁴ and Gang Yang ⁴

¹ School of Materials Science and Engineering, University of Science and Technology Beijing, Beijing 100083, China

² Beijing Mechanical & Electrical Technology Research Institute, Beijing 100083, China

³ School of Materials and Metallurgy, Inner Mongolia University of Science & Technology, Baotou 014010, China

⁴ Institute for Special Steels, Central Iron and Steel Research Institute, Beijing 100081, China

* Correspondence: postustb@163.com (H.Y.); jxdong@ustb.edu.cn (J.D.)

Abstract: Alloys meeting the requirements of “700 °C and above” advanced ultra-super-critical technology, with higher thermal efficiency, have been developed in recent years. Here, a new wrought Ni-based superalloy with excellent high-temperature creep strength based on Waspaloy has been developed and is proposed as a candidate material for application in 700 °C class advanced ultra-super-critical steam turbine blades. In this new alloy, the Molybdenum (Mo) in Waspaloy is partially replaced by Tungsten (W). Creep tests have shown that this new Ni-based alloy has a 70 MPa higher creep-rupture strength than that of Waspaloy at 700 °C by extrapolating the experimental data. Detailed creep-rupture mechanisms have been analyzed by means of scanning electron microscopy, transmission electron microscopy, and chemical phase analysis with a view to devising potential approaches for performance improvements. The results showed that the partial replacement of Mo by W had negligible effect on the composition of carbides precipitated in the alloy. Instead, the amount of the γ' phase was significantly increased, and mismatch between the γ and γ' phases was reduced. In this way, the stability of the γ' phase was increased, its coarsening rate was reduced, and its critical shear stress was increased. As a result, the high-temperature creep-fracture strength of the new alloy was increased.

Keywords: advanced ultra-super-critical; Waspaloy; tungsten; creep-fracture strength; critical shear stress



Citation: Yao, H.; Dong, J.; Gong, Z.; Zhao, J.; Yang, G. Influence of Replacing Molybdenum with Tungsten on the Creep Fracture Property of Waspaloy Nickel-Based Alloy. *Metals* **2022**, *12*, 1842. <https://doi.org/10.3390/met12111842>

Academic Editors: Vera Popovich and Ehsan Hosseini

Received: 16 August 2022

Accepted: 29 September 2022

Published: 28 October 2022

Publisher's Note: MDPI stays neutral with regard to jurisdictional claims in published maps and institutional affiliations.



Copyright: © 2022 by the authors. Licensee MDPI, Basel, Switzerland. This article is an open access article distributed under the terms and conditions of the Creative Commons Attribution (CC BY) license (<https://creativecommons.org/licenses/by/4.0/>).

1. Introduction

In recent years, many countries, including China, have begun to focus on the research and development of advanced ultra-super-critical technology with a steam temperature of 700 °C, whereby the thermal efficiency of power stations is expected to break through the 50% threshold. The extremely harsh service conditions of this grade of power station have led to the development of specifically designed superalloys as candidate materials [1–3].

As the core components of turbine blades, the main candidate materials in various countries are Waspaloy, Nimonic105, USC141, M252, and so on [4,5]. Waspaloy (Ni-20Cr-13Co-4Mo-1.4Al-3Ti-B-Zr), a precipitation-hardening nickel-based superalloy, was developed by Pratt and Whitney in the United States in the 1950s [6] for utilization in aviation engines and power machines. Such alloys are now essential materials for manufacturing turbine disks and blades, showing good tensile and endurance properties below 760 °C and good oxidation resistance above 870 °C. An advantage of Waspaloy is that it has good strength and toughness matching [7].

Waspaloy is mainly used in aero-engine turbine blade materials. M. Razumovskii et al. [8] found that increasing the mass fraction of W would greatly improve the melting temperature of the alloy, and the creep-fracture strength would be more advantageous. Alloying element W can improve the heat resistance of the alloy, but also has the properties of being

cheap, very cost-effective [9]. The Mo content increases the strength and durability of Waspaloy by solid-solution strengthening. A new type of Ni-based alloy has been designed by our research group by partially replacing Mo in Waspaloy with W. The previous study showed that the type of precipitated phases in Waspaloy alloy would not change, and the alloy maintained good structure stability during long-term aging when adding 2% W (mass fraction) to the alloy. Meanwhile, W could refine the size and reduce the growth rate of γ' phase, and improved the tensile strength of the alloy [10–13].

The influence of W on the microstructural stability and properties of such alloys has yet to be fully characterized. Therefore, in this study, we have monitored the effects of long-term aging on carbide separation, precipitation-strengthening phase formation, and the properties of the new alloy. Furthermore, the strengthening mechanism of W substitution of Mo in Waspaloy alloy is discussed.

2. Experimental Material and Procedures

The chemical composition of the test alloy in Table 1 was determined by thermodynamic calculation and combining with the alloys with different W content in the previous study [9,11]. The new alloy (designated as 2Mo2W) was obtained by replacing Mo in Waspaloy with an equal mass of W. The test alloy was melted by a “double-vacuum” process (vacuum induction smelting + vacuum arc remelting), poured into 50 kg ingots, and subsequently forged into a rod of diameter 18 mm. The forging temperature was 1150 °C, the final forging temperature was not lower than 950 °C, and the cooling method is heap cooling. The heat-treatment process involved the following sequential steps: 1080 °C for 4 h (oil cooling), 845 °C for 24 h (air cooling), and 760 °C for 16 h (air cooling). Thereafter, alloy specimens were exposed to 700 °C for 1000–10,000 h or 750 °C for 1000–5000 h in a resistance furnace, then air-cooled to room temperature.

Table 1. Mass percentage compositions of alloys (wt%).

Alloy	C	Cr	Co	Al	Ti	W	Mo	Zr	B	Ni
2Mo2W	0.04	19.49	13.56	1.44	2.95	1.97	2.19	0.028	0.01	Bal.
Waspaloy [14,15]	0.056	19.64	13.68	1.40	3.18	-	4.5	0.044	0.0063	Bal.

The above samples were cleaned with a mixture of CuCl_2 (10 g) + HCl (100 mL) + $\text{CH}_3\text{CH}_2\text{OH}$ (100 mL) or electrolytically etched with HNO_3 (40%) + H_2O (60%) solution. This allowed the microstructures of carbides and the γ' phase to be observed by scanning electron microscopy (SEM, Hitachi S4300, Tokyo, Japan). Qualitative and quantitative analyses of carbides and γ' phase particles were carried out by X-ray diffraction (XRD, APD-10, Milan, Italy; employing $\text{Co-K}\alpha$ radiation and operated at 30 kV and 25 mA) and chemical phase analysis methods. Equilibrium precipitations in the alloys were investigated by thermodynamic calculations using the Ni-9 database.

Two samples were used for each observation, three samples were used for each performance test, performance is averaged over tests.

The creep-fracture strength was tested on the CMT-105 (100 KN) creep test machine, and the samples were $\Phi 5$ mm standard high temperature tensile sample (GB6395-86). The test temperature was 700 °C, and the stresses were 550 MPa, 500 MPa, 475 MPa, 450 MPa, and 425 MPa.

Figure 1 shows the metallographic and scanning microstructure of 2Mo2W and Waspaloy alloys before long-term exposure. The difference of microstructure between the two alloys is not obvious. There are some M_{23}C_6 carbides distributed on the grain boundary. The large precipitations, precipitated in the grain, are unmelted primary MC carbides.

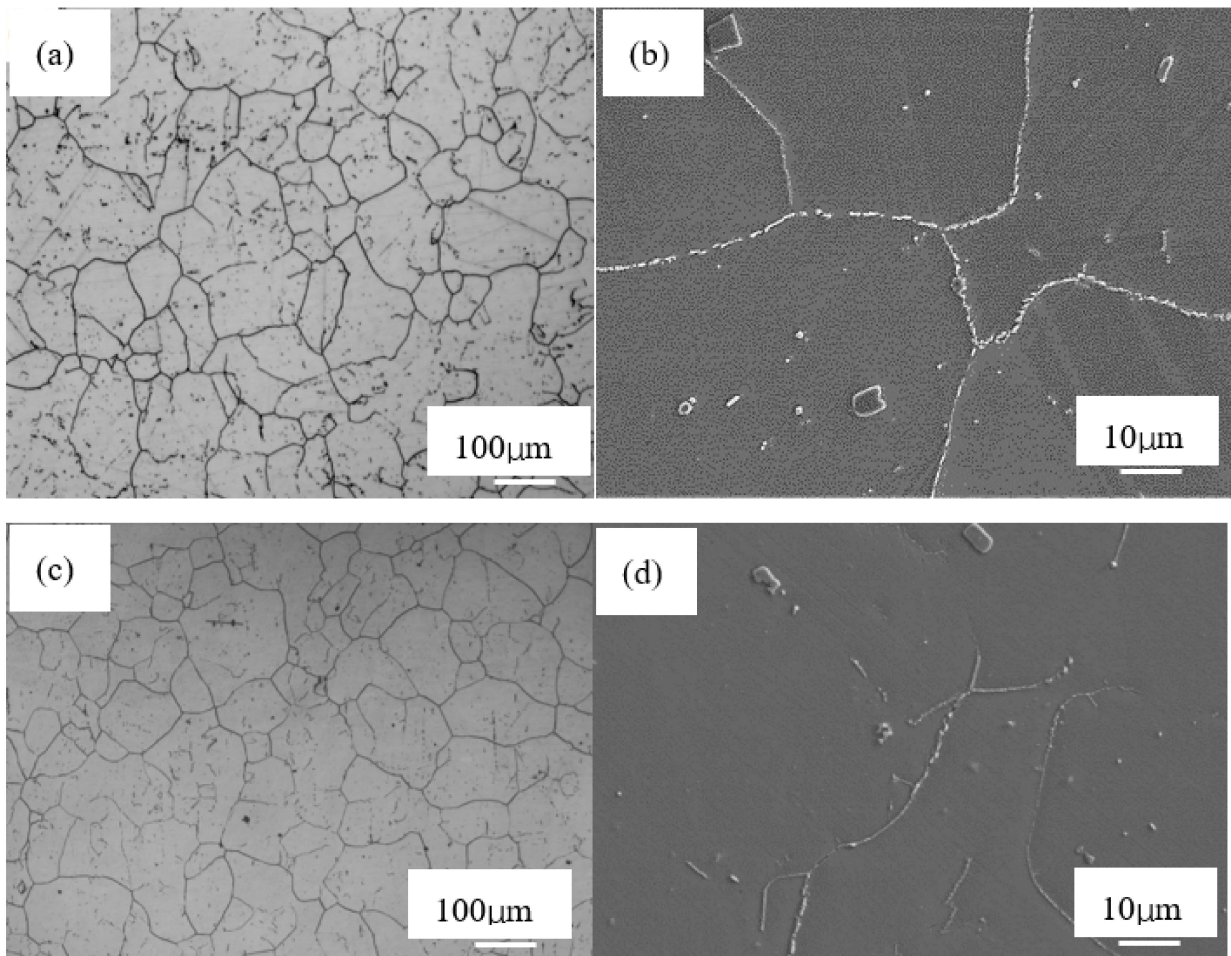


Figure 1. Microstructures of test alloys before long-term exposure. (a,b) Waspaloy; (c,d) 2Mo2W.

3. Results and Discussion

3.1. Characteristics of the Precipitation after Long-Term Exposure

(1) Evolution of carbides

Thermal-CALC thermodynamic software was applied to calculate the equilibrium precipitate composition of the new alloy containing 2% W and 2% Mo, as shown in Figure 2. The precipitate comprised small amounts of the $M_{23}C_6$ phase, MC phase, and μ -phase and a large amount of the γ' phase. Figure 2b shows an enlarged image of the pertinent region of Figure 2a, in which it can be seen more clearly that the $M_{23}C_6$ phase precipitated at 920 °C and then remained almost unchanged with increasing temperature. The μ -phase content increased in a parabolic manner as the sample was cooled, while the γ' phase content increased rapidly.

Thermodynamic calculations can only explain the theoretical equilibrium state, and the actual precipitation process will differ. Figure 3 shows the XRD patterns of the precipitated phase in the alloy before and after long-term aging. From inspection of Figure 3, it can be seen that the carbides in the alloy were $M_{23}C_6$ and TiC both before and after aging. This indicates that long-term aging at 700 °C or 750 °C has no significant effect on the type of carbides precipitated.

No precipitation of σ , τ , or other harmful phases was observed, indicating that their contents were insignificantly small and any effect on the strength of the alloy could be ignored.

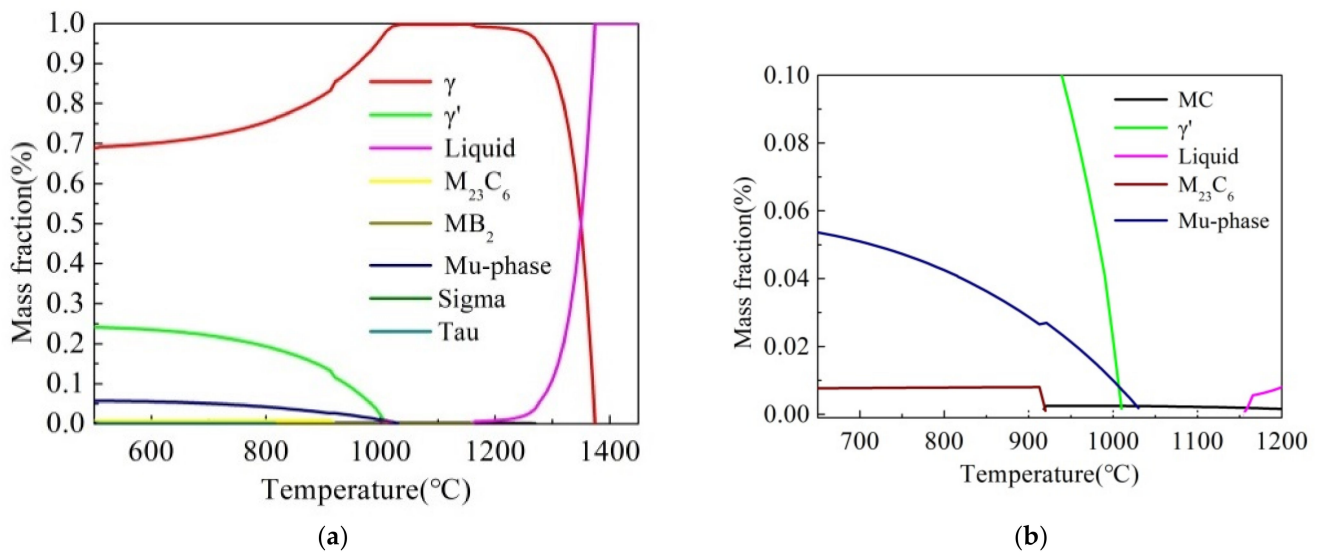


Figure 2. (a). Equilibrium phase diagram of the precipitate in the new alloy; (b) expansion of the pertinent central region in (a).

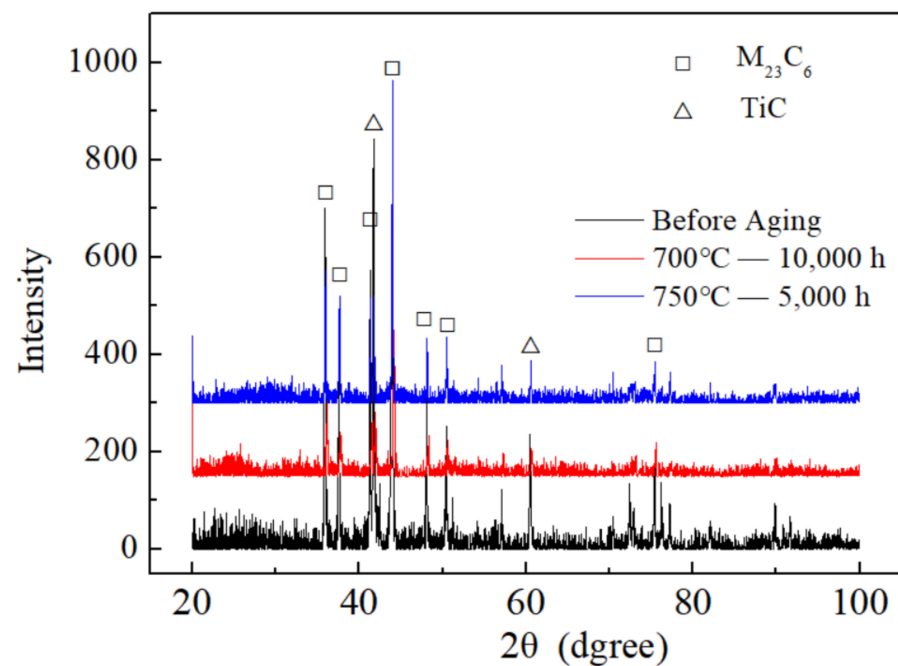


Figure 3. XRD patterns of carbides precipitated in the new alloy before and after long-term aging at different temperatures.

The variations in the contents of $M_{23}C_6$ and MC in the experimental alloy with aging time at 700 °C are shown in Figure 4. The $M_{23}C_6$ content increased steadily with aging time from 0 to 3000 h, reached a maximum at around 5000 h, and thereafter remained essentially unchanged. The MC content slowly increased with aging time from 0 to 3000 h, and thereafter showed a slight decrease.

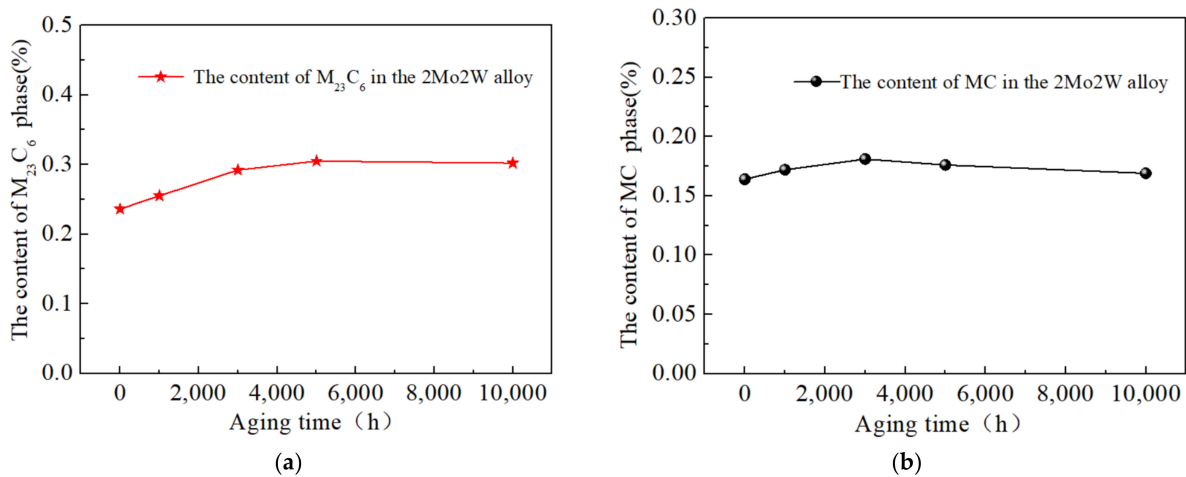


Figure 4. Temporal evolution of the contents of (a) $M_{23}C_6$ and (b) TiC during long-term treatment at 700 °C.

TiC has a high melting point and is usually stable in the range 700–750 °C [16], but during long service of Ni-based alloys, the MC phase will degenerate according to $MC + \gamma \rightarrow M_{23}C_6 + \gamma'$ or $MC + \gamma \rightarrow M_6C + \gamma'$. In some high-W alloys, the $MC + \gamma \rightarrow M_{23}C_6 + \gamma'$ degradation reaction will become $MC + \gamma \rightarrow M_{23}C_6 + \eta$ [17,18]. The η and M_6C phases are not stable and usually have adverse effects on the creep-fracture strengths of alloys.

The MC phase in the long-term aged alloy and its associated precipitation were analyzed by energy-dispersive spectrometry (EDS), and the results are shown in Figure 5 and Table 2.

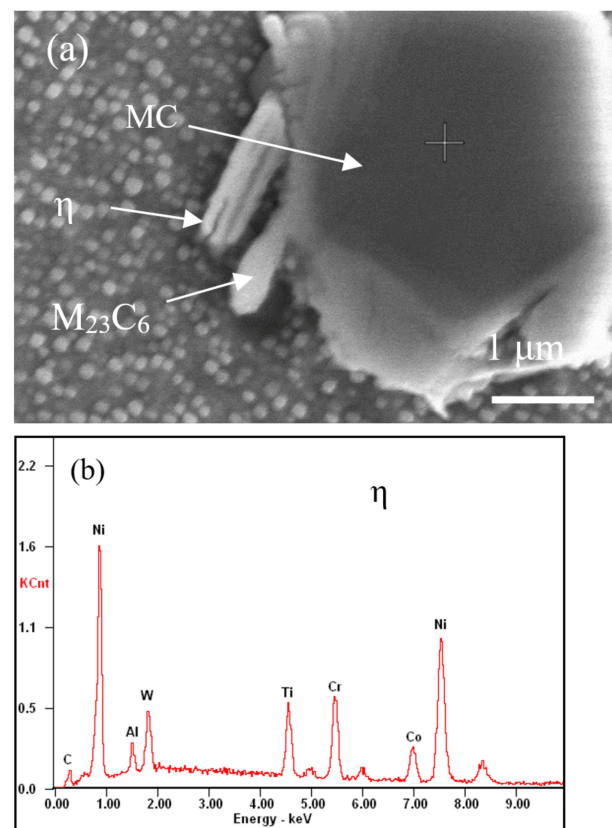


Figure 5. (a) Morphologies of the MC, $M_{23}C_6$ and η phases; (b) EDS of the η phase.

Table 2. Mass percentage compositions of precipitations (wt%).

Precipitation	C K	AlK	WL	TiK	CrK	CoK	NiK	MoL
η	0.04	1.6	1.86	7.17	12.62	11.99	64.72	-
$M_{23}C_6$	2.97	1.49	1.66	3.17	19.03	12.15	56.26	3.27
MC	1.12	0.49	12.35	50.59	8.90	4.65	16.25	6.64

Around the large TiC particles, there are two precipitated phases of two components. Compositional analysis showed one to be the $M_{23}C_6$ phase and the other to be the η phase, rich in Ti [19]. It has been shown previously that, during degradation of the MC phase with high Ti content, the η phase is precipitated. Thus, it can be surmised that the MC phase was degraded here.

(2) Evolution and coarsening kinetics of the γ' phase

Figure 6 shows high-resolution Transmission Electron Microscopy (TEM) images of the interface structure between the γ and γ' phases in the new alloy. From the diffraction pattern in Figure 6b, it can be seen that the γ' particles and the matrix in Figure 6a are both [110] zone axis. Moreover, it can be seen from the enlargement in Figure 6d of the area within the rectangle in Figure 6c that the interface between the γ and γ' phases is a perfect co-lattice, with parallel stripes and no defects such as distortions or dislocations.

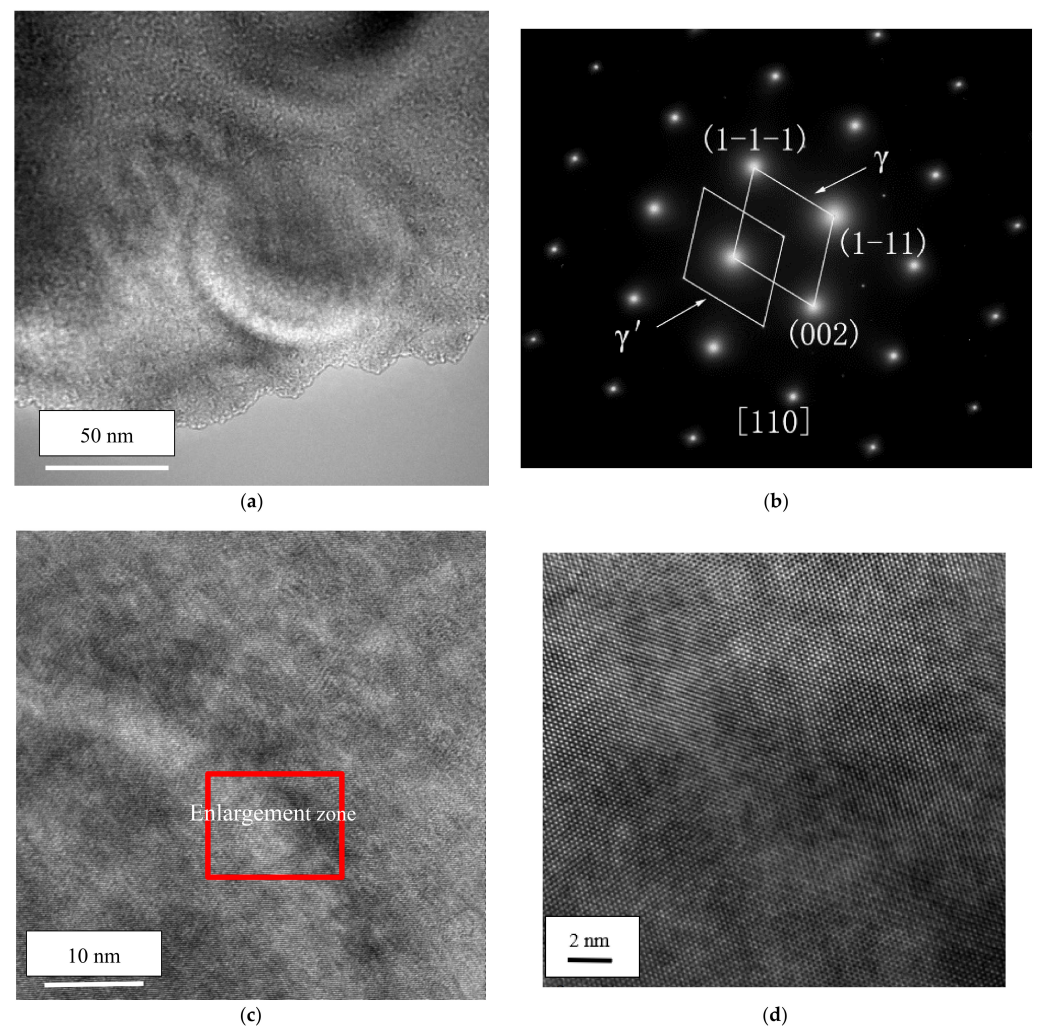


Figure 6. Interface structure between the γ and γ' phases observed by HR-TEM. (a) γ' phase; (b) selected area electron diffraction of γ' ; (c,d) are HR-TEM pictures.

Ostwald ripening coarsening follows the diffusion-controlled particle growth rule: $r^3 \propto t$, where r is the particle size and t is time. In Ni-based superalloys, the coarsening rate can be written as $r^3 - r_0^3 = kt$, where r is the average size of γ' after long-term exposure, r_0 is the average γ' particle size before exposure, and k is the linear coefficient of a plot of $r^3 - r_0^3$ versus exposure time [20,21].

Table 3 shows the size of the γ' phase of test alloys after long-time aging. Figure 7 compares the coarsening rates of the γ' phase in 2Mo2W alloy and Waspaloy over 10,000 h at 700 °C. The coarsening rate of the γ' phase in Waspaloy is $k = 5.76$, more than twice that of the 2Mo2W alloy ($k = 2.47$).

Table 3. γ' phase size of test alloys before and after treatment.

Test Alloy (r/nm)	Before Aging	1000 h	2000 h	5000 h	10,000 h
2Mo2W	30.75	32.15	-	28.90	34.50
Waspaloy	31.40	-	31.80	33.50	41.35

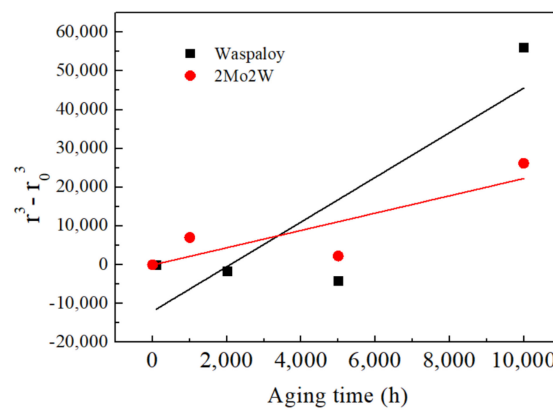


Figure 7. Coarsening rates of 2Mo2W alloy and Waspaloy during long-term aging at 700 °C.

3.2. Discussion on the Mechanism of Creep-Fracture Reinforcement

Figure 8 compares the stress–time enduring logarithmic plots for Waspaloy and the 2Mo2W alloy. Waspaloy has a durable strength of about 340 MPa at 10,000 h, around 70 MPa lower than that of the new alloy.

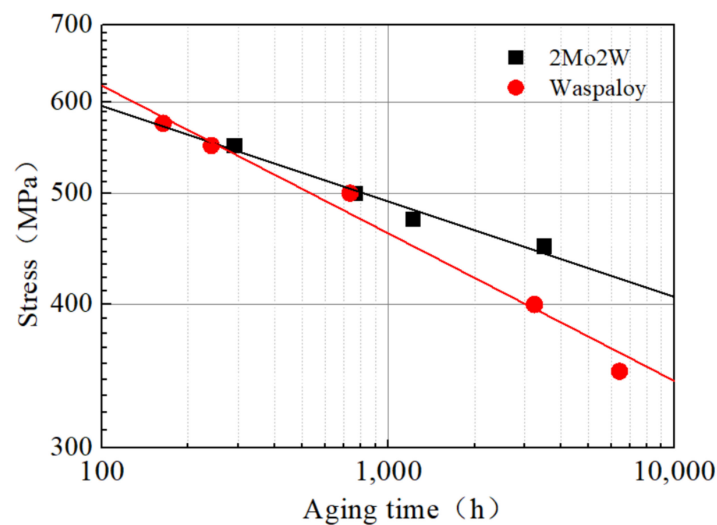


Figure 8. Stress–time creep logarithmic plots for 2Mo2W and Waspaloy.

The strengthening modes of the Ni-based alloy include solid-solution strengthening, γ' -phase precipitation strengthening, and grain boundary precipitation strengthening. To probe the reasons for the creep-fracture strength improvement after replacing Mo with W, the strengths, precipitated phases, and carbide compositions of the two alloys were compared in detail. From Figure 9a,b, one can see the tensile strength, yield strength and hardness of the 2Mo2W alloy before and after aging were higher than those of Waspaloy.

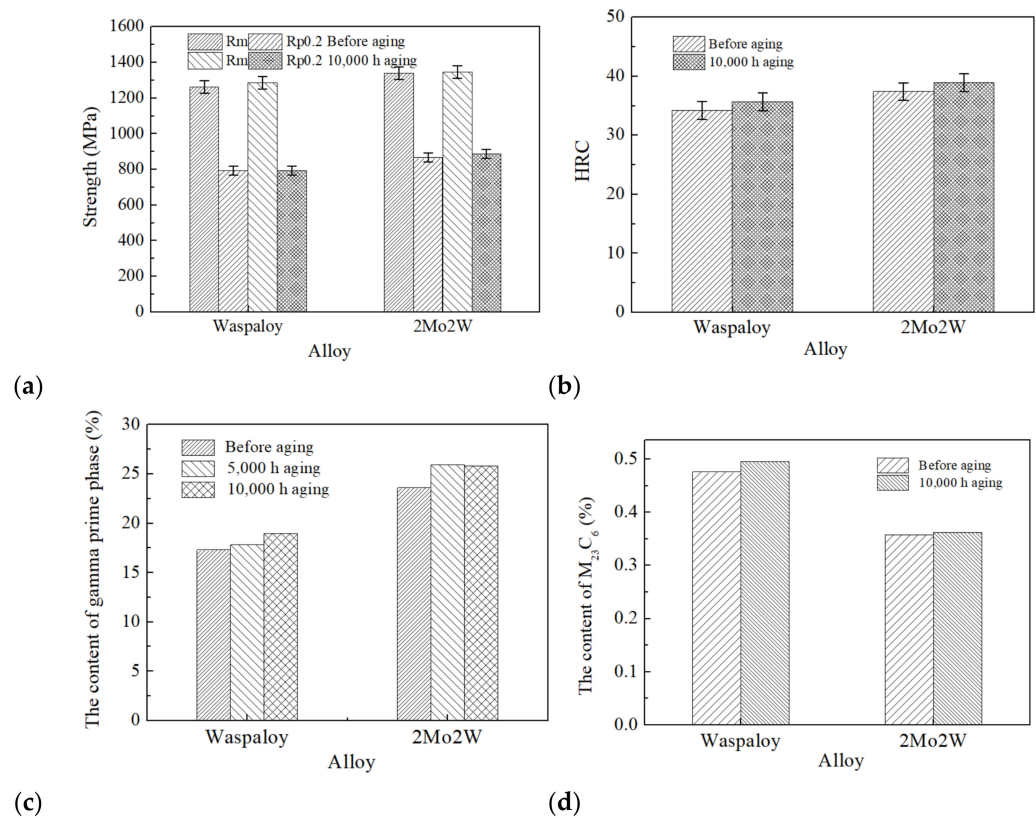


Figure 9. Strengths and precipitate compositions of 2Mo2W alloy and Waspaloy. (a) Strength; (b) Hardness; (c) The content of the γ' phase; (d) The content of $M_{23}C_6$ carbide.

The γ' phase contents of the two alloys prior to aging and after 5000 h and 10,000 h are compared in Figure 9c. The γ' phase content in the 2Mo2W alloy was significantly higher than that in the Waspaloy. After 10,000 h of aging, the γ' phase content of the 2Mo2W alloy was about 5% higher than that of Waspaloy. Figure 9d shows that the $M_{23}C_6$ carbide contents of the two alloys were not significantly different.

Mainly due to the large atomic radius of the added W, additional lattice distortion is generated, which increases the resistance to dislocation motion and increases the solid-solution strengthening effect. Meanwhile, more of the γ' phase leads to an increased precipitation-strengthening effect, imparting the new 2Mo2W alloy with greater strength.

The model of critical shear stress was used to estimate the precipitation-strengthening effect of the γ' phase in the Ni-based alloy, which was mainly estimated by the cutting mechanism or the critical shear stress induced by the bypass mechanism when the γ' phase acts by dislocation.

In the cutting mechanism, for small particles, the weakly coupled dislocation (WCD) model is applicable, whereas for large particles, the strongly coupled dislocation (SCD) model is applicable [22,23].

In both models, the critical shear stress is determined as that required for the edge dislocation pair to cut through the γ' phase along the $\langle 110 \rangle$ direction in the plane (111). In the WCD model, the critical shear stress can be described as:

$$\Delta\tau = \frac{1}{2}A\left(\frac{\Gamma}{b}\right)^{\frac{3}{2}}\left(\frac{bdf}{T}\right)^{\frac{1}{2}} - \frac{1}{2}\left(\frac{\Gamma}{b}\right)f \quad (1)$$

where A is the shape factor of the particle, 0.72 is the value of the spherical particles, Γ is the antiphase domain bounding energy of the γ' phase in the (111) plane, b is the Bergs vector of the edge dislocation in the matrix, and f and d are the volume fraction and diameter of the γ' phase, respectively. T is the linear tension of the dislocation, which can be calculated as follows:

$$T = 0.5Gb^2 \quad (2)$$

where G is the shear modulus, taken as 68 GPa. In the WCD model, the critical shear stress can be described as:

$$\Delta\tau = \frac{1.72}{2}\left(\frac{Tf^{\frac{1}{2}}\omega}{bd}\right)\left(\frac{1.28d\Gamma}{\omega T} - 1\right)^{\frac{1}{2}} \quad (3)$$

where ω is a constant unit.

In the bypass mechanism (Orowan), the critical shear stress can be described as:

$$\Delta\tau = \frac{Gb}{L} \quad (4)$$

where L is the spacing of the nearest neighbor atom, which can be calculated by:

$$L = \frac{2(1-f)d}{3f} \quad (5)$$

In the calculation, Γ was set at 0.28 J/m² and b was set at 0.254 nm. The volume fraction f was taken as 18% for Waspaloy and 25% for 2Mo2W. The calculated data were substituted into the above three models to calculate the corresponding critical shear stresses, as shown in Figure 10.

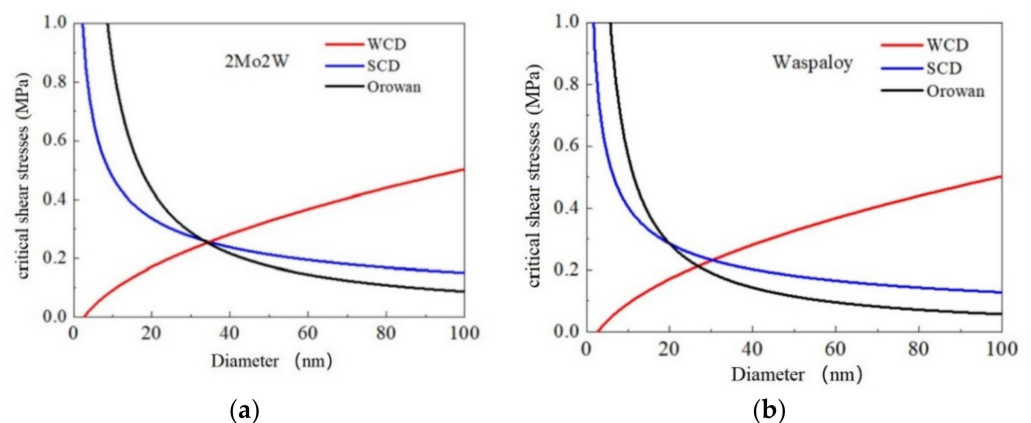


Figure 10. Fitting curves of theoretical critical shear stress versus diameter of the γ' phase for 2Mo2W (a) and Waspaloy (b) at 700 °C.

Given the diameter d of the γ' phase particles, the critical shear stresses corresponding to the three models can be calculated. According to the principle of energy minimization, the dislocation preferentially moves in the direction of least resistance. Therefore, for a given value of d , the actual critical shear stress is the minimum in the three models.

As can be seen from Figure 10, both alloys are dominated by the WCD model when the particles are at their initial size. Figure 10a shows that when 2Mo2W particles grow to about 35 nm, the dislocation bypass model plays a dominant role, and the critical shear

stress at this stage is 0.355 MPa. Figure 10b shows that Waspaloy is similar to 2Mo2W, with only two mechanisms of strong coupling, the dislocation model and the Orowan dislocation bypass model, and the critical shear stress is 0.208 MPa.

Compared with the above results, for the same particle radius of the γ' phase, the critical shear stress of 2Mo2W is larger and the strengthening effect is better. This explains why the increase of the γ' phase content is the main reason for the high creep-fracture strength of 2Mo2W.

The stability of the γ' phase can also affect the creep-fracture performance of Ni-based alloys [24], and the γ' phase coarsening rate and the mismatch degree of the γ' and γ phases (matrix) of the 2Mo2W alloy and Waspaloy were compared.

Small lattice mismatch is beneficial to the creep-fracture properties of the alloy, which is expressed by δ , defined as follows:

$$\delta = 2 \frac{\alpha_{\gamma'} - \alpha_{\gamma}}{\alpha_{\gamma'} + \alpha_{\gamma}} \quad (6)$$

Figure 11 shows the results of dynamics software calculations of the mismatch degrees of the γ and γ' phases in alloys with different W and Mo contents. It can be seen that an alloy with 4% W and no Mo showed the greatest degree of mismatch, followed by an alloy with 4.5% Mo and no W. The least mismatch was seen for the new alloy with 2% W and 2% Mo. This corroborates that the compound addition of Mo and W is conducive to reducing the mismatch of the γ and γ' phases, stabilizing the γ' phase, consistent with the finding that the coarsening rate of the γ' phase of 2Mo2W alloy is lower than that of Waspaloy.

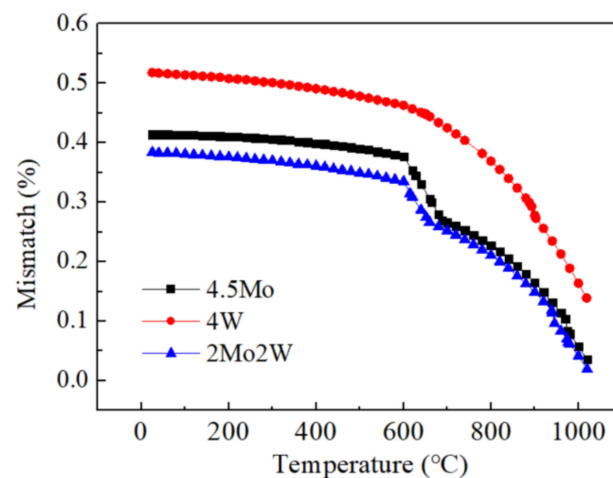


Figure 11. Mismatch of the γ and γ' phases for alloys with different W and Mo contents.

4. Conclusions

A new alloy, designated as 2Mo2W, in which Mo is partially replaced by W, is proposed. During long-term heating of this alloy at 700 °C, the main precipitates that separate have been identified as $M_{23}C_6$ and MC. The creep-fracture strength of 2Mo2W is higher than that of Waspaloy after 10,000 h, which can be mainly attributed to the compound addition of W and Mo, more of the precipitation-strengthening γ' phase, and reduced mismatch of the γ and γ' phases. This renders the γ' phase more stable and lowers the coarsening rate during long-term service at 700 °C. Since the atomic radius of W is larger than that of Mo, its addition reduces the diffusion rates of other alloying elements, increases the stability of the microstructure, and thus improves the creep-fracture strength of the alloy.

Author Contributions: Conceptualization, H.Y. and J.D.; methodology, H.Y. and J.Z.; software, validation, formal analysis, resources, and investigation data curation, H.Y.; writing—original draft preparation, writing—review and editing, H.Y.; supervision, project administration, and funding acquisition, G.Y. and Z.G. All authors have read and agreed to the published version of the manuscript.

Funding: This research was funded by the Inner Mongolia Natural Science Foundation (No. 2022MS05039).

Data Availability Statement: Not applicable.

Conflicts of Interest: The authors declare no conflict of interest.

References

1. Liu, Z.; Chen, Z.; He, X.; Bao, H. Systematical Innovation of Heat Resistant Materials Used for 630~700 °C Advanced Ultra-Supercritical (A-USC) Fossil Fired Boilers. *Acta Metall. Sin.* **2020**, *56*, 539–548. (In Chinese)
2. Du, J.; Lv, X.; Dong, J.; Sun, W.; Bi, Z.; Zhao, G.; Deng, Q.; Cui, C.; Ma, H.; Zhang, B. Research progress of wrought superalloys in China. *Acta Metall. Sin.* **2019**, *55*, 1115. (In Chinese)
3. Abe, F.; Kutsumi, H.; Haruyama, H.; Okubo, H. Improvement of oxidation resistance of 9 mass% chromium steel for advanced-ultra supercritical power plant boilers by pre-oxidation treatment Original Research Article. *Corros. Sci.* **2017**, *114*, 1–9. [[CrossRef](#)]
4. Wang, L.; Yang, G.; Liu, Z.; Wang, L.; Ma, L.; Yang, Z. Effects of Long-term Aging on Microstructure and Mechanical Properties of a Nickel-base Alloy. *Rare Met. Mater. Eng.* **2018**, *47*, 961–967.
5. Peng, T.; Yang, B.; Yang, G.; Wang, L.; Gong, Z. Stress rupture properties and deformation mechanisms of Nimonic 105 alloy at intermediate temperature. *Mater. Sci. Eng. A* **2020**, *777*, 139085. [[CrossRef](#)]
6. Kelekanjeri, V.S.K.G.; Moss, L.K.; Gerhardt, R.A.; Ilavsky, J. Quantification of the coarsening kinetics of γ' precipitates in Waspaloy microstructures with different prior homogenizing treatments. *Acta Mater.* **2009**, *57*, 4658–4670. [[CrossRef](#)]
7. Chamanfar, A.; Jahazi, M.; Gholipour, J.; Wanjara, P.; Yuea, S. Evolution of flow stress and microstructure during isothermal compression of Waspaloy. *Mater. Sci. Eng. A* **2014**, *615*, 497–510. [[CrossRef](#)]
8. Razumovskiy, V.I.; Lozovoi, A.Y.; Razumovskii, I.M. First-principles-aided design of a new ni-base superalloy: Influence of transition metal alloying elements on grain boundary and bulk cohesion. *Acta Mater.* **2015**, *82*, 369–377. [[CrossRef](#)]
9. Bao, H.-S.; Yang, G.; Chen, Z.-Z.; Liu, Z.-D. Effects of long-term aging on microstructure and properties of a tungsten bearing heat-resistant alloy. *J. Iron Steel Res. Int.* **2020**, *27*, 477–487. [[CrossRef](#)]
10. Gong, Z.-H.; Ma, Y.-Y.; Bao, H.-S.; Yang, G. Effect of W on formation and properties of precipitates in Ni-based superalloys. *J. Iron Steel Res. Int.* **2021**, *28*, 910–919. [[CrossRef](#)]
11. Gong, Z.; Bao, H.; Yang, G. Dynamic Recrystallization and Hot-Working Characteristics of Ni-Based Alloy with Different Tungsten Content. *Metals* **2019**, *9*, 298. [[CrossRef](#)]
12. Bao, H.S.; Gong, Z.H.; Chen, Z.Z.; Yang, G. Evolution of precipitates in Ni-Co-Cr-W-Mo superalloys with different tungsten contents. *Rare Met.* **2020**, *39*, 716–724. [[CrossRef](#)]
13. Wang, L.; Yang, G.; Lei, T.; Yin, S.-B.; Wang, L. Hot Deformation Behavior of GH738 for A-USC Turbine Blades. *J. Iron Steel Res. Int.* **2015**, *22*, 1043–1048. [[CrossRef](#)]
14. Wang, L.; Yang, G.; Lei, T.; Yin, S.-B.; Wang, L. Mechanical Properties and Microstructure of Waspaloy Superalloy with W Additions. *Chin. J. Rare Met.* **2016**, *40*, 117–124.
15. Liu, T.F.; Peng, S.W.; Lin, Y.L.; Wu, C.C. Orientation relationships among M23C6, M6C, and austenite in an Fe-Mn-Al-Mo-C alloy. *Metall. Trans. A* **1990**, *21*, 567–574. [[CrossRef](#)]
16. Lvov, G.; Levit, V.I.; Kaufman, M.J. Mechanism of Primary MC Carbide Decomposition in Ni-Base Superalloys. *Metall. Mater. Trans. A* **2004**, *35*, 1669–1679. [[CrossRef](#)]
17. Qin, X.Z.; Guo, J.T.; Yuan, C.; Chen, C.L.; Ye, H.Q. Effects of long-term thermal exposure on the microstructure and properties of a cast Ni-base superalloy. *Metall. Mater. Trans. A* **2007**, *38*, 3014–3022. [[CrossRef](#)]
18. Wang, J.; Zhou, L.; Qin, X.; Sheng, L.; Hou, J.; Guo, J. Primary MC decomposition and its effects on the rupture behaviors in hot corrosion resistant Ni-based superalloy K444. *Mater. Sci. Eng. A* **2012**, *553*, 14–21. [[CrossRef](#)]
19. Wu, X.; Li, Y.; Huang, M.; Liu, W.; Hou, Z. Precipitation kinetics of ordered γ' phase and microstructure evolution in a Ni-Al alloy. *Mater. Chem. Phys.* **2016**, *182*, 125–132. [[CrossRef](#)]
20. Turchi, P.E.A.; Kaufman, L.; Liu, Z.K. Modeling of Ni-Cr-Mo based alloys: Part II—Kinetics. *Comput. Coupling Phase Diagr. Thermochem.* **2007**, *31*, 237–248. [[CrossRef](#)]
21. Brown, L.; Ham, R. *Strengthening Methods in Crystals*; Applied Science Publication Ltd.: London, UK, 1971.
22. Reppich, B.; Schepp, P.; Wehner, G. Some new aspects concerning particle hardening mechanisms in γ' precipitating nickel-base alloys—II. Experiments. *Acta Metall.* **1982**, *30*, 95–104. [[CrossRef](#)]
23. Masoumi, F.; Jahazi, M.; Shahriari, D.; Cormier, J. Coarsening and dissolution of γ' precipitates during solution treatment of AD730™ Ni-based superalloy: Mechanisms and kinetics models. *J. Alloy. Compd.* **2016**, *658*, 981–995. [[CrossRef](#)]
24. Ricks, R.A.; Poter, A.J.; Ecob, R.C. The growth of gamma prime precipitates in nickel-base superalloys. *Acta Metall.* **1983**, *31*, 43–53. [[CrossRef](#)]